Dalton Transactions

Accepted Manuscript

ROYAL SOCIETY OF CHEMISTRY

www.rsc.org/dalton

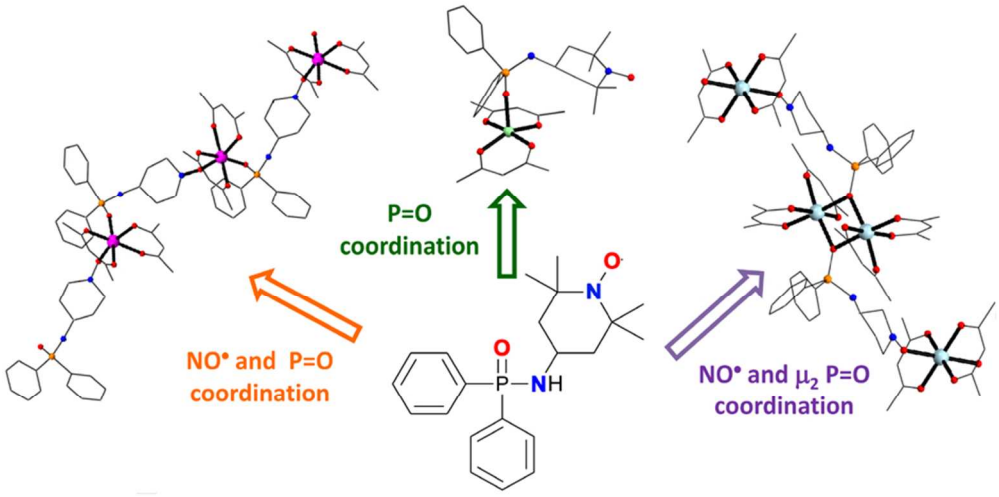

80x39mm (300 x 300 DPI)

TOC Graphic

Synthesis, crystal structures and magnetic behaviour of four coordination compounds constructed by using a phosphinic amide-TEMPO radical and [M(hfac)$_2$] (M=Cu^{II}, Co^{II} and Mn^{II}) building blocks

Samira G. Reis, Miguel A. del Águila-Sánchez, Guilherme P. Guedes, Glaucio F. Braga, Miguel A. Novak, Nivaldo L. Speziali, Fernando López-Ortiz, and Maria G. F. Vaz

The reaction of a phosphinic amide TEMPO radical with [M(hfac)$_2$] building blocks provides discrete or 1D molecular magnetic compounds depending on the coordination mode of the radical.

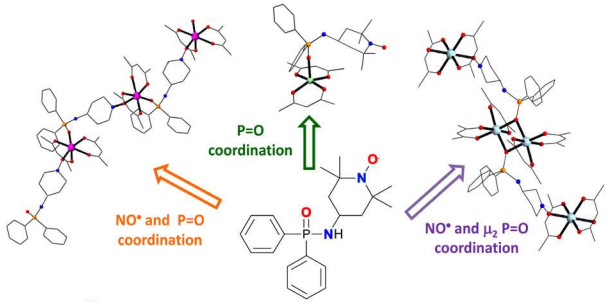

Journal Name

RSCPublishing

ARTICLE

Cite this: DOI: 10.1039/x0xx00000x

Received, XXXX
Accepted XXXX

DOI: 10.1039/x0xx00000x

www.rsc.org/

Synthesis, crystal structures and magnetic behaviour of four coordination compounds constructed by using a phosphinic amide-TEMPO radical and [M(hfac)$_2$] (M=Cu^{II}, Co^{II} and Mn^{II}) building blocks

Samira G. Reis,[a] Miguel A. del Águila-Sánchez,[b] Guilherme P. Guedes,[c] Glaucio F. Braga,[a] Miguel A. Novak,[d] Nivaldo L. Speziali,[e] Fernando López-Ortiz,*[b] and Maria G. F. Vaz*[a]

In the present work we describe the synthesis, crystal structure and magnetic properties of four coordination compounds obtained by assembling a new phosphinic amide containing the TEMPO moiety, 1-piperidinyloxy-4-[(diphenylphosphinyl)amino]-2,2,6,6-tetramethyl radical (dppnTEMPO), with [M(hfac)$_2$] building blocks (M=Cu^{II}, Co^{II}, Mn^{II}). The crystal structures of the coordination compounds revealed the usefulness of the functionalized radical to provide discrete or extended architectures. In the copper compound (**1**) the ligand is coordinated through the oxygen atom of the NP=O linkage to the metal, which exists in square pyramidal or octahedral geometry. For the cobalt and manganese complexes (**2 - 4**), both the phosphinic amide and the nitroxide oxygen atoms are involved in the coordination to the metal leading to one dimensional systems. In the cobalt complex (**2**) an interesting spin topology in the *zig-zag* chain was obtained due to the oxygen atom of the phosphinic amide group is μ_2 coordinated to two cobalt(II) ions. The magnetic behaviour of the coordination compounds shows overall antiferromagnetic interactions involving the metal ion and the organic radical. DFT calculations were performed in order to assign the main path for the magnetic interactions.

1. Introduction

The development of methodologies to design molecular structures with a rational control of the magnetic interactions between the spin carriers has been pursued since the early times of molecular magnetism.[1] One of the successful strategies consists of the assembly of pre-formed paramagnetic building blocks aiming to construct more complex magnetic systems. [M(β-diketonate)$_2$] complexes and organic radicals are representative members of this methodology.[2] The inclusion of these structural fragments into a scaffold can be used to introduce different spins carriers in the same molecule leading to compounds with unusual crystal structures, interesting spin topologies and magnetic properties.[3] Furthermore, a lot of attention has been devoted in the last decade to the synthesis of organic radical-based coordination compounds since the discovery of the first magnetic nanowire, reported by Caneschi and co-authors.[4]

Nitronyl-nitroxides and nitroxides are the organic radicals most used as building-blocks. A number of derivatives were synthesized in order to add new coordination sites beyond the NO moiety, broadening the frontiers towards compounds with remarkable architectures and magnetic properties.[5] Regarding this possibility, a new heterometallic tri-spin system was recently obtained by exploring the hard and soft acidity of the nitroxide moiety or substituent donor atoms.[6] As for the organic radicals used in reactions with block d and/or f metals, those of the nitroxide family are among the most the popular, specially the TEMPO radical (2,2,6,6-tetramethylpiperidine-1-oxyl). Nevertheless, the

employment of phosphorus-based nitroxide derivatives as ligand in the synthesis of molecular magnetic compounds has been little explored. The organophosphorus derivatives of TEMPO investigated to date include phosphates, phosphoramides, thiophosphoramides, phosphonates, selenophosphonates, phosphoramidites and phosphites.[7] Some examples of phosphinic amides bearing an *O*-alkyl-2,2,6,6-tetramethylpiperidin-4-yl moiety have been also reported.[8] The complexation of neutral phosphinic amides with main group elements,[9] transition metals[10] and lanthanides[11] has received little attention. Only a few complexes have been structurally characterized at a molecular level involving mostly chelating ligands.[12,13,14] To the best of our knowledge, the use of phosphinic amide-TEMPO mixed ligands in coordination chemistry remains unexplored. Although the coordination sites of this kind of ligands contains two oxygen atoms, they present different stereoelectronic properties. This characteristic makes the phosphinic amide-TEMPO an interesting building block for accessing to compounds with one-dimensional or unprecedented molecular architectures within the metal-radical strategy. Herein, we report the synthesis of the novel 1-piperidinyloxy-4-[(diphenylphosphinyl)amino]-2,2,6,6-tetramethyl radical, hereafter called as dppnTEMPO (Chart 1), and the synthesis, crystal structures, magnetic properties and DFT calculations for the four coordination compounds obtained through the reaction of $[M(hfac)_2]$ ($hfac^-$ = hexafluoroacetylacetonate and M=Cu^{II}, Co^{II} or Mn^{II}) with this new radical.

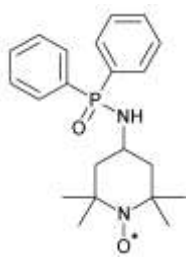

Chart 1. Structure of the dppnTEMPO radical.

2. Experimental Section

2.1. Materials

The synthesis of the radical was carried out in a dry N_2 gas atmosphere using standard Schlenk procedures. THF was distilled from sodium/benzophenone immediately prior to use. Commercial solvents were distilled prior to their use, except *n*-heptane that was used as received. TLC was performed on Merck plates with aluminum backing and silica gel 60 F_{254}. For column chromatography silica gel 60 (40-63 μm) from Scharlau was used. The $[M(hfac)_2]$ building blocks (M= Cu^{II}, Mn^{II} or Co^{II}) were prepared as previously described.[15] NMR spectra were obtained in a Bruker Avance 300 (^{1}H, 300.13 MHz; ^{31}P, 121.49 MHz) using a 5 mm QNP ^{1}H/^{13}C/^{19}F/^{31}P probe. The spectral references used were internal tetramethylsilane for ^{1}H and external 85% H_3PO_4 for ^{31}P. Infrared spectra were recorded in a Bruker Alpha FTIR spectrophotometer. High resolution mass spectra were recorded on an Agilent Technologies LC/MSD TOF instrument using electrospray ionization. Melting point was measured on a Büchi B-540 capillary and PFM II melting point apparatus.

2.2. Synthetic procedures

2.2.1. Synthesis of 1-piperidinyloxy-4-[(diphenylphosphinyl)amino]-2,2,6,6-tetramethyl radical (dppnTEMPO). To a solution of triethylamine (3.6 mL, 25 mmol) and 4-amino-TEMPO free radical (1.71 g, 10 mmol) in THF (40 mL) under N_2 atmosphere at -90 ºC, chlorodiphenylphosphine (1.8 mL, 10 mmol) was added dropwise.[16] The mixture was allowed to warm up gradually to room temperature and was stirred for 2 h. Then, the solution was cooled to -30 ºC and 30% v/v H_2O_2 (1.7 mL, 15.03 mmol) was added and stirred for 1 h more at room temperature. The reaction was poured into a mixture of ice and water and extracted with dichloromethane (3x15 mL). The organic layer was dried over Na_2SO_4 and concentrated under vacuum. The product was purified by flash column chromatography (ethyl acetate:hexane, 4:1 as eluent) affording the dppnTEMPO as pale pink solid. Yield after chromatography 80%. Mp:161-162 ºC. ^{1}H NMR δ ($CDCl_3$, 300.13 MHz) 7.61 (bs, 6H, H3 + H4), 7.80 (bs, 6H, H2) ppm. ^{31}P NMR δ ($CDCl_3$, 121.49 MHz) 25.14 ppm. IR (ATR, υ cm^{-1}) 3175 (bs, NH), 2975 (b), 2937 (b), 1438 (w), 1361 (w), 1302 (w, PN), 1187 (b), 1113 (b), 1082 (b), 907 (w), 723 (b), 695 (w), 645 (w). HRMS (ESI) calcd for $C_{21}H_{28}N_2O_2P$: 371.1888 (M^+), found: 371.1898. The structural assignment was confirmed by adding an equimolecular quantity of phenyl hydrazine to the NMR sample to give *N*-(1-hydroxy-2,2,6,6-tetramethylpiperidin-4-yl)-*P*,*P*-diphenyl-phosphinic amide. ^{1}H NMR δ ($CDCl_3$, 300.13 MHz) 0.91 (s, 6H, H9), 1.10 (s, 6H, H9), 1.49 (t, 2H, $^3J_{HH}$ 12.9 Hz, H7), 1.91 (dm, 2H, $^3J_{HH}$ 11.8 Hz, H7), 2.78 (dd, 1H, $^3J_{PH}$ 5.7 Hz, $^3J_{H,H}$ 10.2 Hz, H5), 3.23 (m, 1H, H6), 7.36 (m, 6H, H3 + H4), 7.80 (dd, 4H, $^3J_{PH}$ 12.1 Hz, $^3J_{HH}$ 1.7 Hz, $^3J_{HH}$ 6.9 Hz, H2). ^{31}P NMR δ ($CDCl_3$, 121.49 MHz) 23.66 ppm.

2.2.2. General synthesis of complexes 1-4. 0.053 mmol of $[M(hfac)_2.nH_2O]$ (M=Cu^{II}, Co^{II} or Mn^{II}) were added to 10 mL of *n*-

heptane and boiled until the complete dissolution of the metal complex. Then, 0.0530 mmol of the dppnTEMPO radical was dissolved in $CHCl_3$ and quickly added under constant stirring. The resulting solution was kept at 10 ºC and after 6-8 days dark-green (M = Cu^{II}) or red crystals (M = Co^{II} or Mn^{II}) were obtained. These crystals were filtered out, washed with *n*-heptane and dried opened to the air. Two kind of single crystals were obtained from the reaction using Co^{II} ions and were labelled as compound **2** and **4**. Since the single crystals have different shapes, they were manually separated. For **1**: *Anal. Calc*. $C_{52}H_{58}CuF_{12}N_4O_6P_2.2(C_{31}H_{30}CuF_{12}N_2O_6P).2(C_7H_{16})$: C, 49.30 %; H, 4.85 %, N, 3.59 %. Found: C 49.13 %; H 4.90 %, N, 3.60 %. IR (ATR, υ cm^{-1}): 3253 (b, NH), 3075 (w), 2983 (w) 2924 (w), 2853 (w) 1640 (m, CO), 1481 (w), 1303 (w, PN), 1253 (s), 1146 (bs), 794 (w), 729 (w), 695 (w), 675 (w). For **2**: *Anal. Calc*. For $C_{72}H_{62}Co_3F_{36}N_4O_{16}P_2.(C_7H_{16})$: C, 41.94 %; H, 3.47 %, N, 2.48 %. Found: C 40.29 %; H 3.53 %, N, 2.75 %. IR (ATR, υ cm^{-1}): 3251 (b, NH), 3065 (w), 2990 (w), 2979 (w), 2938 (w), 2857 (w), 1644 (m, CO), 1485 (b), 1302 (w, PN), 1255 (m), 1142 (bs), 789 (w), 731 (w), 692 (w), 669 (w). For **3**: *Anal. Calc*. For $C_{31}H_{30}F_{12}MnN_2O_6P$: C, 44.30 %; H, 3.60 %, N, 3.33 %. Found: C 44.25 %; H 3.64 %, N, 3.18 %. IR (ATR, υ cm^{-1}): 3427 (sh, NH), 3061 (w), 2986 (w), 2938 (w), 2861 (w), 1650 (m, CO), 1497 (w), 1252 (m), 1185(s), 1139 (bs), 794 (w), 731 (w), 697 (w), 661 (w). For **4**: *Anal. Calc*. For $C_{31}H_{30}F_{12}CoN_2O_6P$: C, 44.09 %; H, 3.58 %, N, 3.32 %. Found: C 43.77 %; H 3.78 %, N, 3.16 %. IR (ATR, υ cm^{-1}): 3417 (b, NH), 2929 (w), 2861 (w), 1645 (m, CO), 1497 (w), 1257 (m), 1190 (s), 1142 (s), 795 (w), 730 (w), 697 (w), 667 (w).

2.3. X-ray diffraction

Single crystal X-ray data of complexes **1-3** were collected on an Oxford GEMINI A Ultra diffractometer using graphite monochromated Mo Kα radiation (λ = 0.71073 Å). Data collection, data reduction, cell refinement and absorption corretions were performed by using the CrysAlis RED, Oxford Diffraction Ltd.,Version 1.171.32.38. For compound **4**, the crystallographic data were collected on a Bruker Enraf-Nonius KAPPA CCD diffractometer using graphite-monochromated Mo Kα radiation (λ = 0.71073 Å) at room temperature. The final unit cell parameters were determined from all reflections obtained with DIRAX program.[17] The integration of the collected reflections was performed using the EVALCCD program.[18] The absorption correction using equivalent reflections was performed with the SADABS program.[19] The structure solutions and refinements were performed with the SHELXS-97 and SHELXL-97 program packages.[20] All atoms except hydrogen were refined anisotropically. The H-atoms were treated by a mixture of independent and constrained refinement. Details of data collection and structure refinement for compounds **1-4** are summarized in Table S1 (Electronic Supplementary Information-ESI). Selected distances are given in Tables 1 (compounds **1** and **2**) and 2 (compounds **3** and **4**). Selected bond angles are summarized in Tables S2 and S3. The ORTEP[21] view of the asymmetric units are depicted in Fig. S1-S4 (ESI).

2.4. DFT calculations

Single point calculations were carried out for compounds **1-4** using the density functional theory method (DFT-B3LYP)[22] in the Gaussian 09W software package.[23] The pseudo-potential LANL2DZ was employed for metals and phosphorus atoms and D95V basis set was implemented to other elements.[24] All results were visualized using Chemcraft.[25] The method to evaluate the magnetic coupling constants and possible path for the magnetic interactions was based on the structural fragmentation according to their charges and multiplicities without any symmetry approximation. The selected detached molecular units in **1-4** present at least one metal ion, coordinated to the $hfac^-$ ligands, and one dppnTEMPO radical. In all systems the fragments were allowed to interact with each other in order to evaluate the intramolecular magnetic coupling in the chains **2-4**, as well as, to study the intermolecular magnetic interaction involving molecules **A** and **B** in **1**. The magnetic coupling constant (*J*) was calculated using Eq (1), through the Broken-Symmetry (BS) approach, where the E_{BS} and E_{HS} terms are the energies of the antiferromagnetic and ferromagnetic spin states, respectively, and S_{max} is the maximum magnetic spin moment value.[26]

$$J = \frac{E_{BS} - E_{HS}}{S^2_{\max}} \qquad \textbf{Eq. (1)}$$

2.5. Magnetic measurements

Variable-temperature magnetic susceptibility and isothermal magnetization measurements were carried out on powdered samples using a Cryogenic SX-600 SQUID (**1-3**) magnetometer or in a Quantum Design PPMS susceptometer (**4**) in the temperature range 2–300 K and field range 0 to 6.5 T. The sample was placed in a gelatine capsule and data were corrected for the sample diamagnetism and sample holder. The magnetic data of compounds **2** and **4** were fitted using the Magprop software, available within the

DAVE package.[27] Details about the calculations are described elsewhere.[28] The mean-field approximation was applied to fit the magnetic data of compounds **2** using the λ parameter, which is related to the intermolecular magnetic interaction through the following equation: $\lambda = J/(g^2\beta^2)$.

3. Results

3.1. Structure descriptions

Compound **1** crystallizes in the monoclinic $P2_1/n$ space group and the molecular structure is shown in Fig. 1. The crystal structure consists of two co-crystallized coordination compounds, namely [Cu(hfac)$_2$dppnTEMPO] (**A**) and [Cu(hfac)$_2$(dppnTEMPO)$_2$] (**B**) and one *n*-heptane crystallization molecule. The two crystallographic independent Cu1A and Cu1B ions are in different coordination environments; in the molecule **A**, the metal ion Cu1A is pentacoordinated to four hfac$^-$ oxygen atoms (O3A, O4A, O5A and O6A) and the phosphinic amide oxygen atom of the dppnTEMPO radical (O2A), lying on a square pyramidal geometry with trigonality parameter τ of 0.01.[29] In molecule **B**, Cu1B ion is on an inversion center and presents an octahedral distorted geometry. The equatorial plane of this ion is formed by four hfac$^-$ oxygen atoms (O3B, O4B, O3B^i and O4B^i; *i*= *-x,-y,-z*) while the axial positions are occupied by O2B and O2B^i phosphinic amide oxygen atoms. In both molecules the Cu-O$_{diketonate}$ bond distances are in good with other reported in the literature.[30] The Cu-O$_{phosphinic\ amide}$ bond lengths are 2.100(3), for Cu1A-O2A, and 2.262(3) Å, for Cu2B-O2B. These bond lenghts are slightly longer when compared with other copper(II) phosphinic amide-based coordination compound.[13f]

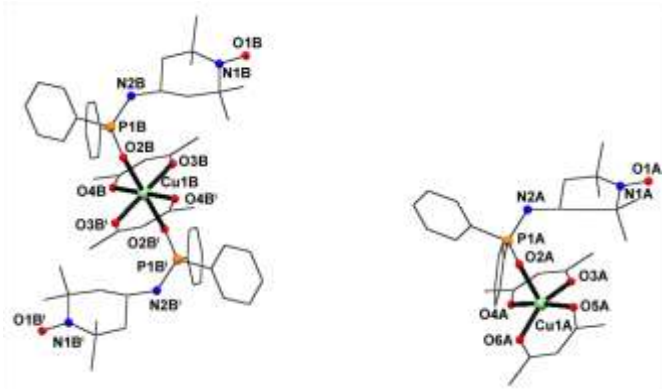

Fig. 1 Molecular structure of the co-crystallized complexes **A** and **B** in compound **1**. Fluorine and hydrogen atoms, as well as, solvent molecules were omitted for the sake of clarity. Symmetry operation to generate equivalent atoms: *i* = *-x, -y, -z*.

Table 1. Selected bond distances (in Å) for compounds **1** and **2**.

1		**2**	
Labels	Bond lengths	Labels	Bond lengths
Cu1B—O4B^i	1.979(2)	Co1—O3	2.030(4)
Cu1B—O4B	1.979(2)	Co1—O4	2.033(4)
Cu1B—O3B	1.983(3)	Co1—O1	2.190(4)
Cu1B—O3B^i	1.983(3)	Co2—O7	2.037(4)
Cu1B—O2B	2.262(3)	Co2—O5	2.044(4)
Cu1B—O2B^i	2.262(3)	Co2—O6	2.065(4)
Cu1A—O3A	1.949(3)	Co2—O8	2.073(4)
Cu1A—O6A	1.952(2)	Co2—O2^i	2.124(3)
Cu1A—O5A	1.956(3)	Co2—O2	2.208(4)
Cu1A—O4A	1.963(2)	N1—O1	1.294(7)
Cu1A—O2A	2.099(3)	N2—P1	1.629(5)
O1A—N1A	1.292(4)	O2—P1	1.524(4)
O1B—N1B	1.291(4)		
O2A—P1A	1.480(3)		
O2B—P1B	1.480(3)		
N2B—P1B	1.631(3)		
N2A—P1A	1.632(3)		

Symmetry operation *i* = *–x,–y,–z*

The coordination of the P=O group to the metal ion does not lead to important modification in the P-O bond lengths [1.480(3) Å in A and 1.486(3) Å in B], when compared with the mean value of 1.484 Å[10c,31] observed for non-coordinated similar phosphinic amide compounds. The same behavior has been found in the P=O bond distance of related phosphine oxide complexes of [Cu(hfac)$_2$].[32] The dppnTEMPO nitroxide moiety remains uncoordinated in all co-crystallized complexes with N-O bond length equal to 1.292(4) Å for N1A-O1A and 1.291(4) Å for N1B-O1B and N1B-O1B^i, which are similar to those observed in other TEMPO derivatives.[33] The shortest intermolecular distance between the metal ions is 10.9919(4) Å (Cu1A···Cu2B^{ii}, *ii*= *½-x, ½+y, ½-z*), whereas the longest one is 17.9392(4) Å. (Cu1A···Cu2B). Concerning the neighbouring uncoordinated nitroxide groups, the intermolecular distances involving both co-crystallized compounds are 6.023(3) Å and 6.110(4) Å, respectively for O1A···O1B^{ii} and O1A^{ii}···O1B (*ii*= *½-x, ½+y, ½-z*). The crystal packing is stabilized by F···F short contacts and a network of hydrogen-bonding involving the nitroxide oxygen atom and the phosphinic amide nitrogen atom [N2A···O1B = 2.848(4) Å and O1A···N2B^{ii} = 2.816(4) Å] in the *ab* plane. These

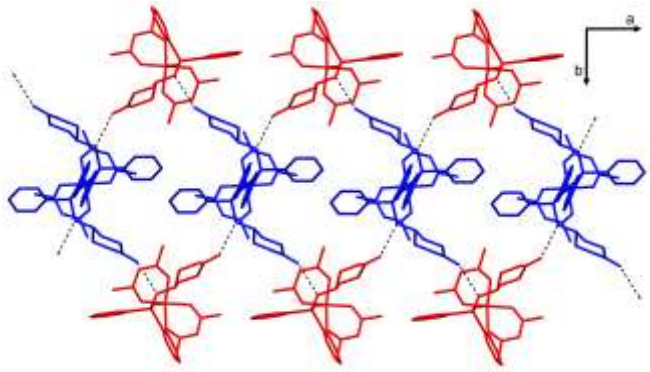

Fig. 2. Details of the crystal packing of compound **1** showing the hydrogen-bonding network. Blue and red colours stand for the molecules **A** and **B**, respectively.

intermolecular interactions lead to supramolecular cavities formed by alternated **A** and **B** molecules, highlighted as red and blue colours (Figure 2). Perpendicular to the *ab* plane, weak intermolecular interactions C_{sp3}-H···O were observed between the hfac$^-$ oxygen atom and the dppnTEMPO methyl groups.

The asymmetric unit of complex **2** contains two crystallographic independent Co^{II} ions coordinated to one radical dppnTEMPO and one *n*-heptane molecule. The molecular structure consists of a *zig-zag* chain, as depicted in Figure 3. The radical plays a key role in order to establish this one-dimensional character, since it acts as bidentade ligand, connecting Co1 and Co2 metal ions. The Co1 ion presents a distorted octahedral geometry, with the axial positions occupied by two nitroxide oxygen atoms (O1 and O1^i, *i* = *-x, -y, -z*), while the basal plane is formed by O3, O3^i, O4 and O4^i hfac$^-$ oxygen atoms. The bond length Co1-O1 is 2.190(4) Å, typically observed for other compounds in which the nitroxide group is coordinated in the same mode to Co^{II} ions.[34] Bond distances in the phosphinic amide moiety are unremarkable.[13] The dppnTEMPO O2 phosphinic amide atom is coordinated to Co2 and Co2^i metal ions in a μ_2 mode. This coordination mode leads to a dinuclear unit within the chain, in which each Co^{II} ion is six-coordinated to two hfac$^-$ and two shared phosphinic amide oxygen atoms. Nevertheless, the hfac$^-$ ligands are *cis* coordinated to Co2 instead of a *trans* configuration observed in Co1 ion. The Co-O bond distances in the phosphinic amide bridges are 2.208(4) Å and 2.124(4) Å, respectively for Co2-O2 and Co2-O2^i, while the Co-O-Co angle is 98.7(2)º. It is important to highlight that the two Co^{II} ions and both dppnTEMPO O2 phosphinic amide atoms are in the same plane. The shortest intrachain distances involving the metal ions are 3.288(1) Å (Co2···Co2^i), 9.887(7) Å (Co1···Co2) and 10.754(7) Å (Co1···Co2^i). Short F···F contacts among

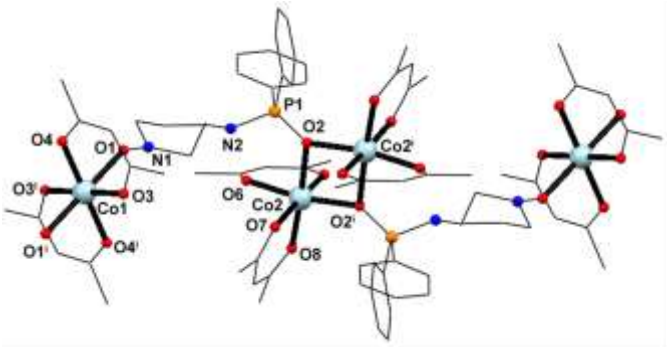

Fig. 3 Fragment of the *zig-zag* chain of compound **2**. Fluorine and hydrogen atoms, methyl dppnTEMPO groups, as well as solvent crystallization molecules were omitted for the sake of clarity. Symmetry operation to generate equivalent atoms: *i* = *-x, -y, -z*.

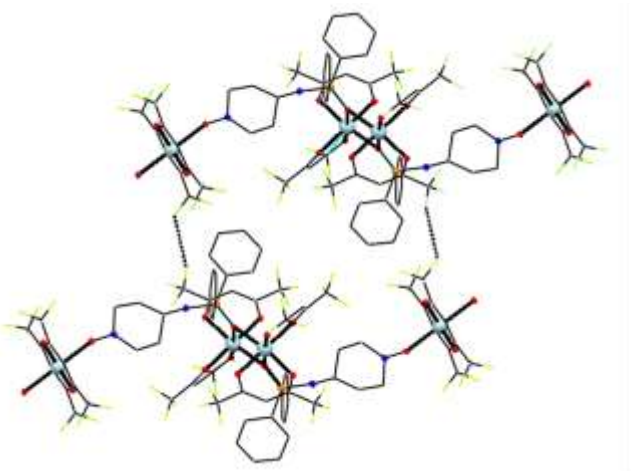

Fig. 4. Details of the crystal packing of compound **2** highlighting the F···F interchain short contacts.

chains stabilize the crystal packing of compound **2**, as seen Figure 4. The structural parameters associated to this contact (F4···F10^i = 2.796(2) Å and angles of 128.1º and 137.7º respectively for ∠C26-F4···F10^i and ∠C31^i-10^i···F4) are in agreement with other parameters reported elsewhere.[35]

Compounds **3** and **4** are isomorphous and crystallize in the tetragonal $I4_1cd$ space group. The fragment of molecular structure of both complexes is depicted in Figure 5. For both compounds, the asymmetry unit contains one crystallographically independent metal ion, which is *cis* coordinated to two hfac$^-$ ligand and one radical.
The dppnTEMPO radical is simultaneously coordinated to two metal ions through the nitroxide and the phosphinic amide groups, with bond lengths M-$O_{phosphinic\ amide}$ = 1.488(1) Å and M-$O_{nitroxide}$ = 1.291(1) Å for **3**, while they are 2.025(2) Å and 2.116(3) Å for **4** respectivelly. This bridging coordination mode leads to a one-

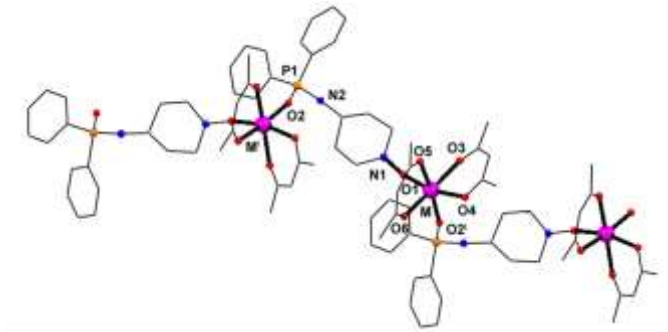

Fig. 5 Fragment of the molecular structure of compounds **3** (M = Mn^{II}) and **4** (M = Co^{II}). Methyl dppnTEMPO groups,fluorine and hydrogen atoms were omitted for sake of clarity.

Table 2. Selected bond distances (in Å) for compounds **3** and **4**.

Labels	**3** (M = Mn^{II})	**4** (M = Co^{II})
M^{i*}—O1	2.105(5)	2.115(4)
M—$O2^{i\perp}$	2.069(5)	2.025(4)
M—O3	2.164(5)	2.083(4)
M—O4	2.198(5)	2.070(4)
M—O5	2.163(5)	2.129(4)
M—O6	2.164(5)	2.060(4)
O1—N1	1.293(7)	1.280(6)
O2—P1	1.488(5)	1.493(4)
N2—P2	1.633(7)	1.641(6)

*For **3**, *i* = *x*,*y*,*z* and for **4**, *i* = *x*, -*y*, ½+*z*
⊥ For **3**, *i* = *x*, -*y*, ½+*z* and for **4**, *i* = *x*,*y*,*z*

dimensional system along the *c* axis. The metal ion in both compounds lies on a distorted octahedral geometry. The geometry of the phosphinic amide functional groups are analogue to other related transition metal complexes.[13]

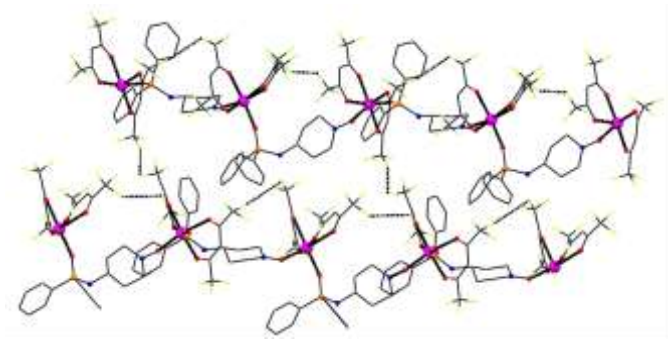

Fig. 6. Details of the crystal packing of compounds **3** (M = Mn^{II}) highlighting the intrachain and interchain short contacts.

The bond angles M-O1-N1 involving the metal ions and the nitroxide moiety are slightly large in the manganese derivative [146.7(4)º] when compared with the cobalt containing compound [143.0(2)º]. The latter angle is equal to the one found for compound

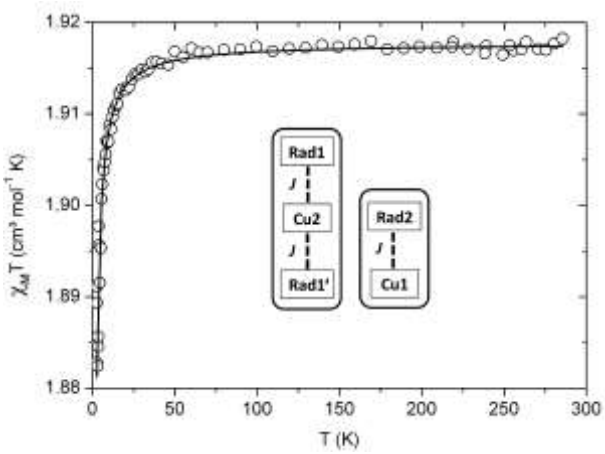

Fig. 7. Thermal dependence of the $\chi_M T$ product for compound **1** at constant magnetic field of 1 kOe. Solid line shows the best fit using Eq. 2 (see text for details). Inset: model of magnetic interactions applied to fit the data. Dotted lines represents the hydrogen bonding as path for the magnetic interactions between the spin carriers.

2, within the experimental error. The shortest intrachain metal-metal distances are 8.871(2) Å and 9.090(2) Å, for compounds **3** and **4,** respectively. In the crystal packing, F···F interactions are present in both compounds. Figure 6 shows these intermolecular contacts for compound **3** (For **3**: $F1\cdots F12^{i}$ = 3.0146(1) Å, ∠C22-F1···$F12^{i}$ = 159.3º and ∠$C31^{i}$-$F12^{i}\cdots$F1=103.9º; F6A···$F9^{i}$ = 3.0183(1) Å, ∠C26-F6A···F9 = 143.7º and ∠$C27^{i}$-$F9^{i}\cdots$F6A=97.9º, *i*=*x*, -*y*, *1/2*+*z*. For **4**: $F2\cdots F12^{i}$ = 3.07(1) Å, ∠C22-F2···F12 = 113.3º and ∠$C31^{i}$-$F12^{i}\cdots$F2=168.1º; F6···F7A = 3.07(2) Å, ∠C26-F6···F7A = 127.8º and ∠C27-F7A···F6=124.9º, *i*=*x*, -*y*, *1/2*+*z*).

3.2. Magnetic Properties

The thermal dependence of the $\chi_M T$ product for compounds **1**-**3** is shown in Figures 7-9. For **1**, the $\chi_M T$ value at room temperature is *c.a.* 1.92 $cm^3 \cdot mol^{-1} \cdot K$, which is close to the calculated value (1.87 $cm^3 \cdot mol^{-1} \cdot K$) for two noninteracting copper(II) ions (S = 1/2) and three nitroxide radicals (S = 1/2) with g = 2.00. This value remains nearly constant in the temperature range of 300 to 40 K, and upon cooling $\chi_M T$ decreases to 1.88 $cm^3 \cdot mol^{-1} \cdot K$ indicating antiferromagnetic interactions. The reciprocal susceptibility *versus* temperature can be fitted to the Curie-Weiss law [χ_M= C/(T-θ)], giving a Curie and Weiss constants of C = 1.89 $cm^3 \cdot mol^{-1} \cdot K$ (0.38 $cm^3 \cdot mol^{-1} \cdot K$ for each S=1/2) and θ = –0.13 K (see Fig. S5, ESI). The antiferromagnetic interaction among the spin carriers are very weak. In fact, the intramolecular distances between the nitroxide oxygen

atom and the Cu^{II} ions are large, being 7.7879(2) Å and 8.1319(2) Å in molecules **A** and **B**, respectively. Thus, the magnetic interaction involving these magnetic centers is expected to be very weak since the organic radical is not directly coordinated through the N-O moiety to the metal ion. In addition, the spin carriers are separated through a sp^3 carbon skeleton, which does not allow a significant spin delocalization within the co-crystallized molecules. Another possible path for the magnetic interactions would be through the intermolecular hydrogen-bond between the molecules **A** and **B**. A careful analysis on this intermolecular contact showed that the distance between the magnetic centers of neighboring molecules is shorter than the intramolecular one. The intermolecular path was chosen for further analysis by DFT calculations, as will be discussed later. It is important to stress that a simplified model with one coupling constant was used to describe the magnetic behaviour since the proposed path was the same in both units with similar distances between the spin carriers (~ 6.3 Å). Besides, if two magnetic coupling constants were used, the experimental uncertainity of J increases strongly, leading to a meaningless result. The magnetic data were reproduced considering a sum of the magnetic susceptibility of dinuclear system with [$H = -J(\vec{S}_{Cu1} \cdot \vec{S}_{Rad2})$] plus a linear magnetic trimer [$H = -J(\vec{S}_{Cu2} \cdot \vec{S}_{Rad1} + \vec{S}_{Cu2} \cdot \vec{S}_{Rad1}')$] (Eq 2).[36] The subscripts 1 and 2 represent the metal ions or radicals from the **A** or **B** molecules, respectively (see inset figure 7) and S_{Cu}=S_{rad} = 1/2.

$$\chi_M T = \frac{Ng^2\beta^2}{k}\left\{\frac{2}{[3+\exp(-J/kT)]} + \frac{1}{4}\left[\frac{1+\exp(J/kT)+10\exp(3J/2kT)}{(1+\exp(J/kT)+2\exp(3J/2kT)}\right]\right\}$$

Eq. (2)

The best fit was achieved with g = 2.02 and J = –0.11(1) cm^{-1} (solid line in figure 7). This result is consistent with the large intermolecular distance between the Cu^{II} ion and the nitroxide moiety (~ 6.3 Å) observed in both dinuclear and trinuclear supramolecular magnetic units.

The magnetization versus field curve obtained at 1.8 K is depicted in Figure S5 (ESI). At a magnetic field of 65 kOe, the magnetization reaches a maximum of 5.0 Bohr magneton, which is expected for five non-interacting spins S = 1/2 (two Cu^{II} ions with g > 2.00 and three nitroxide radical with g = 2). These data could be

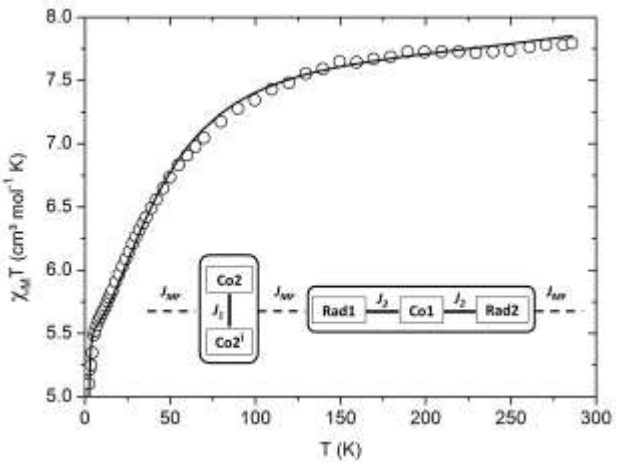

Fig. 8.Thermal dependence of the χ_MT product for compound **2** at constant magnetic field of 1 kOe. Solid line shows the best fit. Inset: model of magnetic interactions applied to fit the data (see text for details).

nicely described by a sum of five Brillouin function S=1/2[37], calculated considering g = 2.05 (see solid line in Fig. S6, ESI).

The crystal structure of compound **2** consists of a one-dimensional system containing two magnetic units isolated by the sp^3 carbon skeleton of the radical: i) a Co^{II} dimer, in which the metal ions are bridged coordinated through the phosphinic oxygen atom, and ii) a magnetic trimer formed by two radicals and one Co^{II} ion. Based on this structural feature the magnetic data for compound **2** were treated considering these two magnetic units. The χ_MT x T curve is shown in Figure 8. The χ_MT value[37] of one octahedral Co^{II} is tipically 3.2 $cm^3 \cdot mol^{-1} \cdot K$ at room temperature, so considering three non-interacting Co^{II} ions plus two nitroxide radicals, the calculated χ_MT value is 10.3 $cm^3 \cdot mol^{-1} \cdot K$, much higher than the experimental value (7.8 $cm^3 \cdot mol^{-1} \cdot K$). This large difference evidences that strong antiferromagnetic interactions are already opperative at this temperature. Lowering the temperature, χ_MT decreases continuously to 5.1 $cm^3 \cdot mol^{-1} \cdot K$ at 2.0 K due to predominant antiferromagnetic interactions among the spin carriers and zero field splitting effects of Co^{II} ions. The Curie-Weiss law fit in temperature range of 50-300 K gives a Curie and Weiss constants of C = 8.1 $cm^3 \cdot mol^{-1} \cdot K$ and θ = –10 K (see Fig. S7, ESI). In order to account for the magnetic interactions in **2**, a simplified model with two exchange interactions and a mean-field approximation was used to fit the data (see Fig. 8) using the following the spin Hamiltonian (Eq. (3)).

$$H = -J_1(\vec{S}_{Co2} \cdot \vec{S}_{Co2i}) - J_2(\vec{S}_{Co1} \cdot \vec{S}_{Rad1} + \vec{S}_{Co1} \cdot \vec{S}_{Rad2})$$

Eq. (3)

In this equation, J_1 represents the magnetic interaction between the two Co^{II} ions within the dinuclear unit, while J_2 stands for the magnetic coupling involving Co^{II} ion and nitroxide radicals in the trimer. In addition, an axial single-ion zero field splitting term parameter (DS_z^2) for the Co^{II} ions, as well as a mean field (MF) approximation to quantify the magnetic interactions between the units (J_{MF}) were added to the model. The best fit (solid line Fig. 8) was achieved with g_{Co} = 2.70(1), g_{rad} = 2.00 (fixed), J_1 = –0.72(1) cm^{-1}, J_2 = –504(8) cm^{-1}, J_{MF} = –0.30(1) cm^{-1} and D = 50.9(2) cm^{-1}. The bridging angle between the Co^{II} ions in the dinuclear unit, nearly 98º in **2**, is expected to give rise to a weak antiferromagnetic interaction, as observed in other Co^{II} compounds.[38] The strong antiferromagnetic interaction within the triad radical-Co^{II}-radical are also in agreement with typical values for magnetic coupling constants obtained for cobalt-nitroxide complexes described by Caneschi and co-workers (> 300 cm^{-1}).[39] In comparison with cobalt-nitronyl nitroxide complexes, the strongest magnetic coupling constant obtained for **2** can be justified by the fact that the spin density in the dppnTEMPO radical is generally located over the nitrogen and oxygen atoms when compared with nitronyl nitroxide derivatives, whose spin density are delocalized along the O-N-C-N-O fragment.[34] It is also important to highlight that no acceptable fit could be obtained down to low temperatures without taking into account the intermolecular magnetic interactions (J_{MF}). Finally, the axial zero-field splitting parameter value is in the range observed for distorted octahedral cobalt(II) ions.[40]

The field dependence of the magnetization at 1.8 K for compound **2** reaches an almost saturated value of 8.0 Bohr magnetons at a magnetic field of 65 kOe (Fig. S8. ESI). As Co^{II} ions behave as an effective spin S' = 1/2 with an anisotropic $g \approx 3.5$ below 30 K,[41] this value is consistent with two isolated Co ions and the strongly antiferromagnetic triad Rad-Co-Rad.

The magnetic data of the manganese derivative **3** are shown in Figure 9. At room temperature strong antiferromagnetic interactions between manganese and the nitroxide radical are operative, since the experimental $\chi_M T$ value at 285 K is 3.3 $cm^3 \cdot mol^{-1} \cdot K$, much lower than calculated spin-only value for one manganese (S = 5/2) and one nitroxide radical (S = 1/2), with g = 2.00 (6.0 $cm^3 \cdot mol^{-1} \cdot K$). Cooling the sample, $\chi_M T$ value decreases smoothly until 3.05 $cm^3 \cdot mol^{-1} \cdot K$ at 20 K. This value is close to a S = 2 state expected for isolated Mn^{II} ion antiferromagnetically coupled to the nitroxide radical. Below

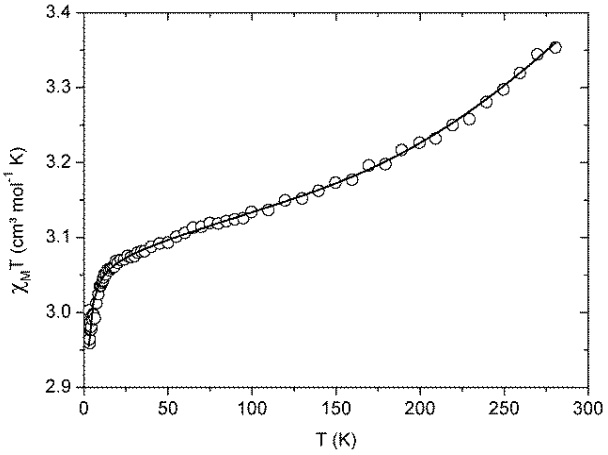

Fig. 9.Thermal dependence of the $\chi_M T$ product for compound **3** at constant magnetic field of 1 kOe. Solid line shows the best fit (see text for details).

20 K, the decrease of the $\chi_M T$ can be attributed to weak intermolecular antiferromagnetic interactions. The reciprocal susceptibility *versus* temperature was fitted to the Curie-Weiss law leading to a Curie and Weiss constants of C = 3.28 $cm^3 \cdot mol^{-1} \cdot K$ and θ = –1.8 K (see Fig. S9, ESI). Although compound **3** crystallizes as a 1D framework, the magnetic data were reproduced by a simplified model, considering an isotropic interaction between one manganese and one nitroxide radical [$H = -J(\vec{S}_{Mn} \cdot \vec{S}_{Rad})$] and a mean field approximation (Eqs. 4 and 5)[42] in order to account for the weak magnetic interactions between Mn-Rad dimers *via* sp^3 carbon skeleton of the dppnTEMPO radical.

$$\chi_m = \frac{N\beta^2 g^2}{kT}\left[\frac{28+10\exp(-6J/kT)}{7+5\exp(-6J/kT)}\right] \quad \textbf{Eq. 4}$$

$$\chi_m^{MF} = \frac{\chi_m}{1-zJ_{MF}\chi_m} \quad \textbf{Eq. 5}$$

Solid line in Figure 9 shows the best fit achieved with J = –120(8) cm^{-1}, zJ_{MF} = –0.040(2) cm^{-1} and g = 2.01(1). The J value is in good agreement when compared with similar compounds in which the oxygen atom of the nitroxide group is coordinated to a manganese(II) ion.[43] The weak magnetic interaction between Mn-Rad dimers *via* sp^3 carbon skeleton is comparable with that obtained for compound **2**. The low temperature magnetization for **3** (see Fig. S10, ESI) shows saturation magnetization value of 4.1 Bohr magnetons as expected for a S = 2 Mn^{II}-dppnTEMPO radical antiferromagnetic dimer. The magnetic data could be well described

by the a $S = 2$ Brillouin function with $g = 2.04$ (solid line in Fig. S10, ESI).

The thermal dependence of the $\chi_M T$ product for compound **4** is depicted in Figure 10. The room temperature $\chi_M T$ value is 2.0 $cm^3 \cdot mol^{-1} \cdot K$, which is lower than the expected for one octahedral Co^{II} ion and one nitroxide radical, indicating that strong antiferromagnetic interactions are operative at this temperature. Upon cooling, the $\chi_M T$ value decreases continuously to 0.3 $cm^3 \cdot mol^{-1} \cdot K$ at 2 K due to predominant antiferromagnetic interactions and zero field splitting of Co^{II} ions. Compound **4** presents a similar structure to the manganese derivative, so the magnetic data can also be treated as a Co-Rad magnetic dimer, since the magnetic interactions between these magnetic units through the sp^3 carbon atoms of the radical is expected to be very weak, as seen for **3**. The magnetic data were reproduced by using the following spin Hamiltonian $H = -J(\vec{S}_{Co} \cdot \vec{S}_{Rad})$ and an axial single-ion zero field splitting term parameter (DS_z^2) for the Co^{II} ion. Specifically for compound **4**, no acceptable fit could be achieved by including a mean field approximation at low temperatures: an unrealistic moderate ferromagnetic interaction is found between the Co-Rad dimers. Recall that from the manganese(II) derivative **3**, this magnetic interaction would be expected to be weak and antiferromagnetic. This difference in the magnetic behavior of compound **4** is explained by the fact that at low temperatures the Co^{II}-Rad dimer has a much lower effective spin, with $\chi_M T$ near 0.3 $cm^3 \cdot mol^{-1} \cdot K$. Similar magnetic behavior was found in the $Co_2(hfac)_4(RL)_2$ compound (RL=5-(3-(N-tert-butyl-N-aminoxyl)phenyl)pyrimidine radical), which forms dimers of S=1 units (S_{Co}-S_{rad}).[44] Actually the magnetization curve *versus* field (Fig. S11 – ESI) presents low magnetization values at 2 K compatible with a strong AF dimer with small effective moment and large anisotropy (smooth increases up to 70 kOe). The χ_M^{-1} x T curve (Fig. S12 – ESI) shows at low temperatures a deviation from the Curie-Weiss law below 60 K. The fit in the temperature range 80-300 K leads to C = 2.40 $cm^3 \cdot mol^{-1} \cdot K$ and $\theta = -55$ K. In order to fit the data in the whole temperature range, a paramagnetic contribution (ρ) ne eded to be added. This kind of contribution is often found in many antiferromagnetic dimers and is usually attributed to isolated monomers and/or crystal defects. The solid line in Figure 10 represents the best fit achieved with $g_{Co} = 2.50(1)$, $g_{rad} = 2.00$ (fixed), $J = -505(6)$ cm^{-1}, $D = 99.9(1)$ cm^{-1} and $\rho = 0.07$. The magnetic coupling

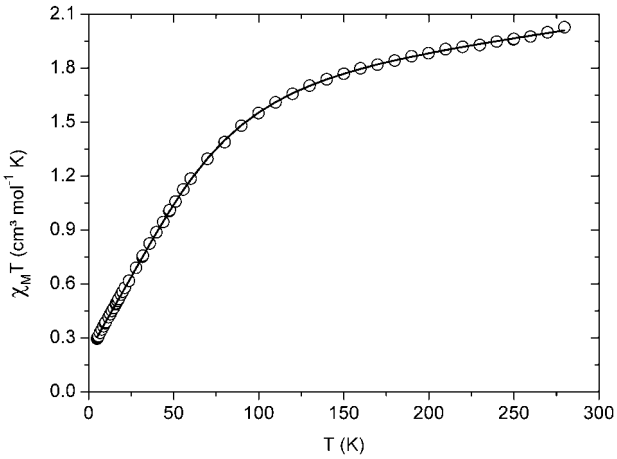

Fig. 10.Thermal dependence of the $\chi_M T$ product for compound **4** at constant magnetic field of 2 kOe. Solid line shows the best fit (see text for details).

constant and the axial zero-field splitting parameter values are in agreement with the range values reported in the literature.[39,40] It is important to note that the obtained antiferromagnetic coupling constant value for the Co-Rad dimer in compound **4** is equal to that previously described for **2** in the triad Rad-Co-Rad. Note that the magnetic coupling constant is stronger in the cobalt(II) derivative **4** than in the manganese(II) containing compound **3** which is consistent with other reports on magnetic properties of isomorphous compounds containing a nitroxide moiety coordinated to these metal ions.[34,43a]

3. DFT calculations

Broken-symmetry method has been widely used for evaluation of magnetic couplings for systems that exhibit single or multiple magnetic interaction in extended systems.[45] However, more accurate calculations of J can be achieved with multireference methods, which necessarily presents an extremely high computational cost depending on the system dimension, such as in case of compounds **1**-**4**.[46] The use of these methods goes beyond the scope of our work, since our goal was to perform a qualitative evaluation of the electronic and magnetic properties. The DFT calculations, discussed hereafter, were performed to support the model of interactions used to fit and assign the most probable path for the magnetic coupling between the spin carriers in the magnetic system described in this work.

3.1. Co-crystallized compounds 1

In order to study the intramolecular and intermolecular magnetic interactions within the co-crystallized molecules **A** and **B** (see Fig. 11), the E_{HS} and E_{BS} energies were calculated for both fragments separately. The results show that the antiferromagnetic state is 0.0525 cal·mol^{-1} more stable than the ferromagnetic one. The spin density for each Cu^{II} is 0.67 in **A** and 0.71 in **B**, with small spin delocalization involving the $hfac^-$ oxygen atoms. In the dppnTEMPO moiety this density is concentrated in the NO group with 0.96 in **A** and **B**. The coupling constants involving the Cu^{II} ion and dppnTEMPO radical in the separated fragments are nearly zero (-0.004 cm^{-1} for **A** and -0.002 cm^{-1} for **B**) indicating that in both fragments the metal ion and the radical are magnetically well isolated, *i.e.*, the overall magnetic behavior of **1** could not be considered as the sum of the magnetic response of a magnetic dimer (unit **A**) and a magnetic trimer (unit **B**). A simplified model containing both molecules **A** and **B** was used to describe the supramolecular arrangement and evaluate the role of the hydrogen-bonding network as a path for the intermolecular magnetic interactions between Cu1 and Rad2 in these co-crystallized compounds. The magnetic coupling constant (J_{int}) was found found to be -0.04 cm^{-1}, with a S = 2 ground state (see spin density map shown in Figure 11). This J_{int} value is ten times higher than those previously found for the isolated **A** and **B** fragments, indicating that the hydrogen-bonding interactions are the most probable path of the magnetic interactions in compound **1**. Although the calculated J_{int} value is underestimated for this simplified model in comparison to the experimental one (J_{MF} = –0.11 cm^{-1}), both values are in the same order of magnitude. Table S4 summarizes the results of the energies of each state associated with compound **1** in different multiplicities.

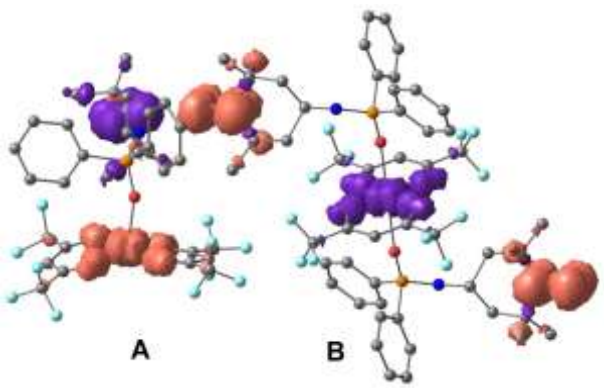

Fig. 11. Spin density map of **1** for the co-crystallized molecules (A+B). The contour value is 0.004 a.u.

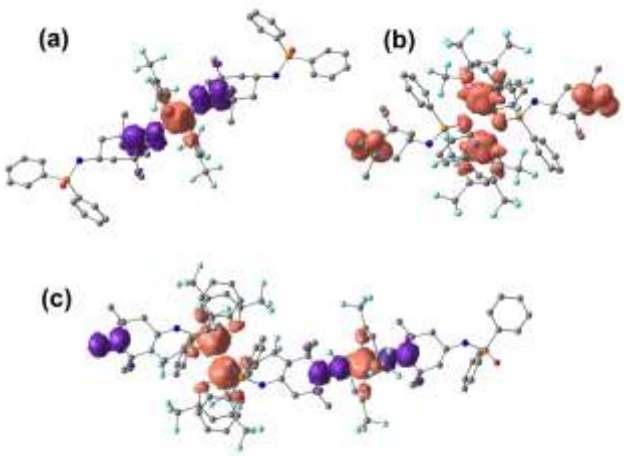

Fig. 12. Spin density maps for fragments i (a), ii (b) and the supermolecule i+ii (c) used to compute the magnetic properties of compound **2**. The contour value is 0.004 a.u. for all representations

3.2. Compound 2

As discussed for the copper compound, the intramolecular magnetic interaction *via* the piperidinyl ring is expected to be very weak.[47] This feature simplifies the DFT study of compound **2** by considering that it is formed by two isolated magnetic units within the chain, namely: (i) one magnetic trimer Rad-Co1-Rad and (ii) one Co2-Co2^i dimer. An evaluation of the multiplicity was carried out in both units and revealed that the multiplicity S = 2 is the ground state for fragment (i), while the septet state is the most stable for the Co_2 unit (ii). Figure 12 shows the spin density maps for the most stable multiplicity states in both units. Table S5, shows the energies of each state associated with compound **2** in different multiplicities. The spin density of the Co^{II} ions in fragments (i) and (ii) are 2.79 and 2.72, respectively, with a small spin delocalization towards $hfac^-$ oxygen atoms. In the fragments (i) and (ii), the spin density in the nitroxide moiety is 0.97. These results for (i) confirmed the antiferromagnetic coupling observed between the metal ion and the axially coordinated nitroxide group, but were not able to describe the antiferromagnetic interaction in the dinuclear Co^{II} unit. The calculated J values are –304.7 cm^{-1} and 0.5 cm^{-1}, respectively for isolated (i) and (ii) units. Although the calculated J value in fragment (i) is small in comparison with the experimental one, it clearly shows the nature of the magnetic interactions. However, a very weak ferromagnetic coupling is predicted by DFT calculations for fragment (ii). The differences observed can be justified by the fact that the magnetic data were fit taking into account the axial zero-field splitting parameter, D, which were neglected in the DFT study. The change in

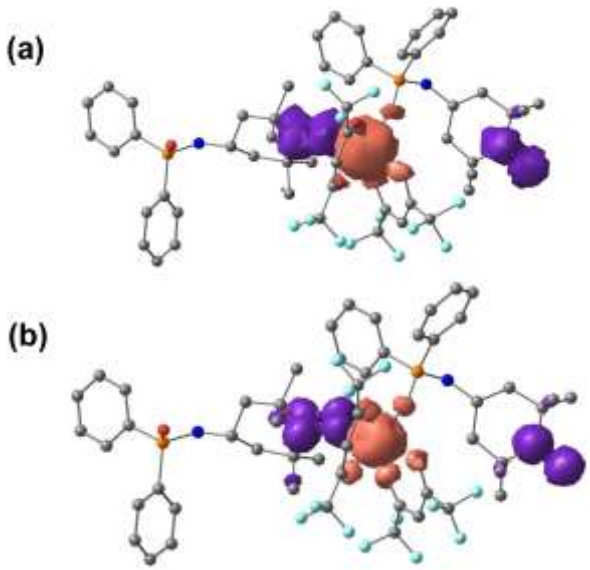

Fig. 13. Spin density maps of the antiferromagnetic ground state for the fragment chain for compounds **3** (a) and **4** (b). The contour value is 0.004 a.u for all representations.

the sign of the coupling in (ii) as compared with the experimental data can be ascribed to the inaccuracy in reproducing very weak effects computationally. Similar results are obtained when the computed system includes both the Co2 core and the Rad-Co-Rad moiety, as can be seen in the supermolecule depicted in Figure 12c (See Table S5 for energy values). Importantly, the strongest antiferromagnetic interaction is adequately predicted. The magnetic interactions within the chain were modelled by accounting for the magnetic coupling between the dinuclear Co_2 and the trimeric Rad-Co-Rad units (i) and (ii). The calculations revealed an antiferromagnetic interaction with J_{int} of -6.2 cm^{-1} (see Fig. 12c for the spin density map), which is overestimated as compared with the experimental value. The results of the DFT study indicate that the calculations reproduce qualitatively the magnetic properties observed for **2** and confirmed the spin topology found in the chain.

3.3. Compounds 3 and 4

DFT calculations were carried out using a fragment of the chain $[M(hfac)_2(dppnTEMPO)_2]$ ($M=Mn^{II}$, for **3**, or Co^{II}, for **4**) as model system. This specific unit was selected in order to understand the magnetic coupling between the dppnTEMPO radicals coordinated to the metal ion through the nitroxide and the phosphinic amide groups within the chain. For both compounds the ground state was found to

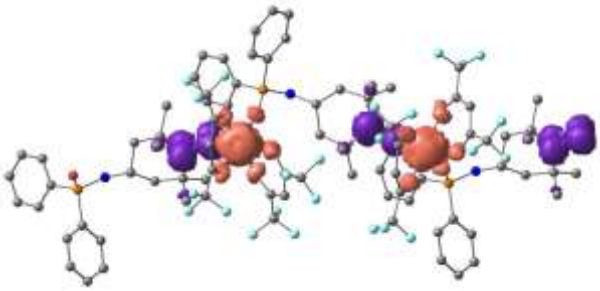

Fig. 14. Spin density maps in the antiferromagnetic ground state for the supermolecule of compound **3**. The contour value is 0.004 a.u.

be antiferromagnetic, as shown in Figure 13. In the manganese compound, the spin density over the Mn^{II} ion is 4.78, with small spin delocalization towards coordinated $hfac^-$ oxygen atoms and phosphinic amide group (*c.a.* 0.02 for each coordinated atom). The dppnTEMPO radical involved in its coordination sphere has a spin density of 0.58 and 0.40 respectively in the nitroxide oxygen and nitrogen atoms. The dppnTEMPO radical connected to the metal ion by the phosphinic amide oxygen atom has the spin density also located over the N-O group (0.54 and 0.43, for N and O, respectively). A similar analysis performed on the cobalt compound **4** afforded the following spin density values: i) 2.74 for the Co^{II} ion, with a spin delocalization towards the coordinated oxygen atoms (*c.a.* 0.04 for each coordinate atom); ii) 0.37 and 0.56 respectively in the oxygen and nitrogen atoms for the nitroxide group coordinated to the metal ion; and iii) 0.53 (O) and 0.45 (N) for the uncoordinated nitroxide group belonging to the second radical (see Fig. 13b). For the manganese derivative, a strong antiferromagnetic interaction between the metal ion and the dppnTEMPO radical coordinated through the nitroxide group was found (J = -107.4 cm^{-1}). This value is in good agreement with the experimental data (-120 cm^{-1}). The DFT calculations also revealed that the second dppnTEMPO radical (coordinated by the phosphinic amide group to the metal ion) is weakly antiferromagnetically coupled to the previously discussed unit, with a J_{int} of -0.02 cm^{-1}. This value is similar to that obtained by the fit of the magnetic data. Importantly, this weak magnetic interaction proved to be essential for achieving a reasonable fit of the experimental data at low temperatures. Therefore, the results of the computational study support the model of interactions used for describing the magnetic properties of **3**.

In compound **4**, the ground state is also a result of the antiferromagnetic interactions between the metal ion and the dppnTEMPO coordinated by the nitroxide group, with a calculated magnetic coupling constant of -107.2 cm^{-1}. This antiferromagnetic

behaviour is expected for this kind of compound in which the nitroxide group is axially coordinated to the Co^{II} ion.[48] Nevertheless, the magnetic interaction would be stronger in the Co^{II} derivative than in the Mn^{II} compound, as reported previously for isotructural nitroxide containing coordination compounds.[34] This variation can be explained due to the additional complications caused by the spin-orbit coupling present in the cobalt compound. In a similar way to the manganese derivative, the magnetic interaction between the cobalt ion and radical coordinated through the oxygen phosphinic amide atom is weakly antiferromagnetic, with $J_{int} = -0.05$ cm^{-1}.

Finally, in order to investigate the one-dimensional character of compounds **3** and **4**, a supermolecule containing two metal ions and three radical, $[M_2(hfac)_4(dppnTEMPO)_3]$ was also calculated. In this new situation, the magnetic coupling constant between the metal ion and the radical coordinated through the nitroxide moiety is smaller than those obtained for isolated units, but it still represents the main contribution to the overall magnetic properties of these compounds ($J = -73.8$ cm^{-1} for **3** and $J = -55.0$ cm^{-1} for **4**). The spin density map for **3** is depicted in Figure 14. The results of the DFT study indicate that the calculations reproduce qualitatively the magnetic properties observed and confirmed the spin topology found in the chain. Tables S6 and S7, shows the energies of each state associated with compounds **3** and **4** in different multiplicities.

4. Conclusions

In this work we described the synthesis, characterization and magnetic properties of four coordination compounds based on a new phosphinic amide TEMPO derivative radical, 1-piperidinyloxy-4-[(diphenylphosphinyl)amino]-2,2,6,6-tetramethyl (dppnTEMPO). The crystal structures of the compounds of Cu^{II}, Mn^{II} and Co^{II} showed that this rather simple bidentate ligand is a valuable scaffold for the construction of different molecular architectures consisting of discrete molecules and chains. This structural diversity proceeds from the presence in the molecule of two different oxygen-based coordination sites, a phosphinic amide and a nitroxide radical. The magnetic studies revealed overall antiferromagnetic interactions within the compounds and the magnetic data were fitted using simplified models, since the magnetic interactions between the spin carriers are weak, as expected by considering the sp^3 carbon skeleton of the dppnTEMPO radical as an interaction path. The choice of the model of interactions was supported by DFT calculations with the broken-symmetry approach, which allowed to assign the path for the magnetic interactions in compounds **1**-**4** as well as qualitatively account for the magnetic coupling constant values.

Supporting Information

Crystallographic data for compounds **1**-**4** in CIF format are available as CCDC-No. 997015 to 9917018. These data can be obtained free of charge from The Cambridge Crystallographic Data Centre via www.ccdc.cam.ac.uk/data_request/cif. Figures S1-S4 display the ORTEP view of the asymmetric unit of compounds **1**-**4**. Figures S5-S12 contain the field dependence of the magnetization and Curie-Weiss plots for compounds **1**-**4**. Summary of the crystal structure, data collection and refinement for compounds **1**-**4** are shown in Table S1. Selected bond angles are listed in Tables S2 and S3. The absolute energies and the Δ_{Energy} obtained by DFT calculations are summarized in Tables S4-S7.

Acknowledgements

The authors acknowledge the financial support from CAPES, FAPERJ, CNPq, MINECO and FEDER (project CTQ2011-27705). The authors thank LABCRI (Universidade Federal de Minas Gerais), LDRX and LMQC (Universidade Federal Fluminense).

Notes and references

[a]Instituto de Química, Universidade Federal Fluminense, 24020-141 Niterói, RJ, Brazil. Email: mariavaz@vm.uff.br

[b]Área de Química Orgánica, Universidad de Almería, Crta. Sacramento s/n, 04230, Almería, Spain

[c] Instituto de Ciências Exatas, Departamento de Química, Universidade Federal Rural do Rio de Janeiro, 23870-000 Seropédica, RJ, Brazil

[d] Instituto de Física, Universidade Federal do Rio de Janeiro, 21941-972 Rio de Janeiro, RJ, Brazil

[e] Departamento de Física, Universidade Federal de Minas Gerais, 31270-901 Belo Horizonte, MG, Brazil

1 (*a*) Y. Pei, Y. Journaux, O. Kahn, A. Dei and D. Gatteschi, *J. Chem. Soc., Chem. Commun.*, 1986, 1300; (*b*) Y. Pei, M. Verdaguer, O. Kahn, J. Sletten and J.-P. Renard, *J. Am. Chem. Soc.*, 1986, **108**, 7428; (*c*) D. Gatteschi, *Advan. Mater.*, 1994, **6**, 635; (*d*) R. Gheorghe, P. Cucos, M. Andruh, J.-P. Costes, B. Donnadieu and S. Shova, *Chem. Eur. J.*, 2006, **12**, 187; (*e*) E. Pardo, R. Ruiz-Garcıa, J. Cano, X. Ottenwaelder, R. Lescouëzec, Y. Journaux, F. Lloret and M. Julve, *Dalton Trans.*, 2008, 2780; (*f*) R. Sessoli, A. K. Powell, *Coord. Chem. Rev.*, 2009, **253**, 2328; (*g*) T. B. Faust, V. Bellini, A. Candini, S. Carretta, G. Lorusso, D. R. Allan, L. Carthy, D. Collison, R. J.

Docherty, J. Kenyon, J. Machin, E. J. L. McInnes, C. A. Muryn, H. Nowell, R. G. Pritchard, S. J. Teat, G. A. Timco, F. Tuna, G. F. S. Whitehead, W. Wernsdorfer, M. Affronte and R. E. P. Winpenny, *Chem. Eur. J.*, 2011, **17**, 14020; (*h*) C. Train, M. Grusellec and M. Verdaguer, *Chem. Soc. Rev.*, 2011, **40**, 3297.

2 (*a*) C. Rajadurai, V. Enkelmann, V. Ikorskii, V. I. Ovcharenko, and M. Baumgarten, *Inorg. Chem.*, 2006, **45**, 9664; (*b*) M. V. Fedin, E. G. Bagryanskaya, H. Matsuoka, S. Yamauchi, S. L. Veber, K. Yu. Maryunina, E. V. Tretyakov, V. I. Ovcharenko, and R. Z. Sagdeev*; J. Am. Chem. Soc.*, 2012, **134**, 16319; (*c*) Y. Numata, K. Inoue, N. Baranov, M. Kurmoo and K. Kikuchi, *J. Am. Chem. Soc.*, 2007, **129**, 9902; (*d*) M. G. F. Vaz, R. A. A. Cassaro, H. Akpinar, J. A. Schlueter, P. M. Lahti, M. A. Novak, *Chem. Eur. J.* 2014, **20**, 5460.

3 (*a*) M. V. Fedin, K. Y. Maryunina, R. Z. Sagdeev, V. I. Ovcharenko and E. G. Bagryanskaya, *Inorg. Chem.*, 2012, **51**, 709; (*b*) X.-L. Mei, R.-N. Liu, C. Wang, P.-P. Yang, L.-C. Li and D.-Z. Liao, *Dalton Trans.*, 2012, **41**, 2904; (*c*) S. L. Veber, M. V. Fedin, K. Y. Maryunina, A. Potapov, D. Goldfarb, E. Reijerse, W. Lubitz, R. Z. Sagdeev, V. I. Ovcharenko and E. G. Bagryanskaya, *Inorg. Chem.*, 2011, **50**, 10204; (*d*) G. V. Romanenko, K. Y. Maryunina, A. S. Bogomyakov, R. Z. Sagdeev and V. I. Ovcharenko, *Inorg. Chem.* 2011, **50**, 6597; (*e*) Y.-Z. Zhang, D.-F. Li, R. Clérac and S. M. Holmes, *Polyhedron*, 2013, **64**, 393.

4 A. Caneschi, D. Gatteschi, N. Lalioti, C. Sangregorio, R. Sessoli, G. Venturi, A. Vindigni, A. Rettori, M. G. Pini, M. A. Novak, *Angew. Chem. Int. Ed.* 2001, **40**, 1760.

5 I. Ratera and J. Venciana, *Chem. Soc. Rev.*, 2012, **41**, 303.

6 M. Zhu, X. Mei, Y. Ma, L. Li, D. Liao and J.-P. Sutter, *Chem. Commun.*, 2014, **50**, 1906.

7 For recent references see: (*a*) S. Iwamoto, W. Kai, T. Isogai, T. Saito, A. Isogai and T. Iwata, *Polym. Degrad. Stab.*, 2010, **95**, 1394; (*b*) H. Moons, E. Goovaerts, V. P. Gubskaya, I.A. Nuretdinov, C. Corvajac and L. Franco, *Phys. Chem. Chem. Phys.*, 2011, **13**, 3942; (*c*) B. Huras, J. Zakrzewski and M. Krawczyk, *Heteroatom Chem.*, 2011, **22**, 137; (*d*) V. Bansal, Y. Delgado, M. D. Legault and G. Barletta, *Molecules*, 2012, **17**, 1870; (*e*) C. H. Wunderlich, R. G. Huber, R. Spitzer, K. R. Liedl, K. Kloiber and C. Kreutz, *ACS Chem. Biol.*, 2013, **8**, 2697.

8 R. Pfaendner, M. Roth, K.-U. Schoening, T. Weiss and S. B. Hindalekar, PCT (BASF, Germany), 2011, WO 2011086114.

9 (*a*) M. W. G. de Bolster and W. L. Groeneveld, Z. *Naturforsch. B*, 1972, **27**, 759; (*b*) I. Y. Kuramshin, S. S. Bashkirov, A. A. Muratova, R. A. Manapov, A. S. Khramov and A. N. Pudovik, *Zh. Obshch. Khim.*, 1975, **45**, 701; (*c*) I. Fernández, J. González and F. López-Ortiz, *J. Am. Chem. Soc.*, 2004, **126**, 12551.

10 (*a*) P. O. Dunstan, G. Vicentini and Y. Kawano, *An. Acad. Bras. Cienc*. 1974, **46**, 23; (*b*) B. Faure, O. Pardigon and G. Buono, *Tetrahedron*, 1997, **53**, 11577; (*c*) C. Popovici, P. Oña-Burgos, I. Fernández, L. Roces, S. García-Granda, M. J. Iglesias and F. Lopez-Ortiz, *Org. Lett.*, 2010, **12**, 428.

11 Selected examples: (*a*) G. Vicentini and P. O. Dunstan, *J. Inorg. Nucl. Chem.*, 1971, **33**, 1749; (*b*) G. Vicentini and J. C. Prado, *J. Inorg. Nucl. Chem.*, 1972, **34**, 1309; (*c*) L. B. Zinner, G. Vicentini and L. Rothschild, *J. Inorg. Nucl. Chem.*, 1974, **36**, 2499; (*d*) L.B. Zinner and G. Vicentini, *Inorg. Chim. Acta*, 1975, **15**, 235; (*e*) G. Vicentini and L. C. Machado, *J. Inorg. Nucl. Chem.*, 1981, **43**, 1676; (*f*) J. R. Matos, L. B. Zinner, K. Zinner, G. Vicentini and P. O. Dunstan, *Thermochim. Acta*, 1993, **219**, 173.

12 Main group metal complexes: (*a*) A. M. Arif, A. H. Cowley, R. M. Kren and D. L. Westmoreland, *Heteroatom Chem.*, 1990, **1**, 117; (*b*) M. Nieger, G. David and E. Niecke, Private communication, 2001, CCDC 174118; (*c*) I. Fernández, R. D. Price, P. D. Bolton, M. F. Mahon, M. G. Davidson and F. López-Ortiz, *J. Organomet. Chem.*, 2004, **689**, 1890; (*d*) K. Naktode, R. K. Kottalanka, S. K. Jana and T. K. Panda, *Z. Anorg. Allg. Chem.*, 2013, **639**, 999.

13 Transition metal complexes: (*a*) H. Wang, H. Shen, H.-S. Chan and Z. Xie, *Organometallics*, 2008, **27**, 3964; (*b*) C.-W. Yeh and J.-D. Chen, *Inorg. Chem. Commun.*, 2011, **14**, 1212; (*c*) A. Malassa, B. Schulze, B. Stein-Schaller, H. Görls, B. Weber and M. Westerhausen, *Eur. J. Inorg. Chem.*, 2011, **2011**, 1584; (*d*) B. Bichler, L. F. Veiros, O. Oztopcu, M. Puchberger, K. Mereiter, K. Matsubara and K. A. Kirchner, *Organometallics*, 2011, **30**, 5928; (*e*) C. Holzhacker, C. M. Standfest-Hauser, M. Puchberger, K. Mereiter, L. F. Veiros, M. J. Calhorda, M. D. Carvalho, L. P. Ferreira, M. Godinho, F. Hartl and K. Kirchner, *Organometallics*, 2011, **30**, 6587; (*f*) C.-W. Yeh, K.-H. Chang, C.-Y. Hu, W. Hsu and J.-D. Chen, *Polyhedron*, 2012, **31**, 657.

14 Lanthanide complexes: (*a*) E. E. Castellano, G. Oliva, J. Zuckerman-Schpector, G. Vicentini and L. R. F Carvalho, *Inorg. Chim. Acta*, 1985, **109**, 33; (*b*) A. R. de Aquino, G. Bombieri, P. C. Isolani, G. Vicentini and J. Zukerman-Schpector, *Inorg. Chim. Acta*, 2000, **306**, 101; (*c*) E. I. Matrosov, I. B. Goryunova, K. A. Lysenko, M. S. Grigor'ev, A. M. Safiulina, E. I. Goryunov and E. E. Nifant'ev, *Russ. J. Inorg. Chem.*, 2011, **56**, 539; (*d*) A. G. Matveeva, T. V. Baulina, Z. A. Starikova, M. S. Grigor'ev, Z. S. Klemenkova, S. V. Matveev, L. A. Leites, R. R. Aysin and E. E. Nifant'ev, *Inorg. Chim. Acta*, 2012, **384**, 266; (*e*) K. Gholivand and H. R. Mahzouni, *Inorg. Chim. Acta*, 2012, **386**, 8.

15 E. W. Berg and J. T. Truemper, *J. Phys. Chem.*, 1960, **64**, 487.

16 (*a*) I. Fernández, F. López-Ortiz, B. Tejerina and S. García-Granda, *Org. Lett.*, 2001, **3**, 1339; (*b*) I. Fernández, F. López-Ortiz, A. Menéndez-Velázquez and S. García-Granda, *J. Org. Chem.*, 2002, **67**, 3852.

17 A. J. M. Duisenberg, *J. Appl. Crystallogr.*, 1992, **25**, 92.

18 A. J. M. Duisenberg, L. M. J. Kroon-Batenburg and A. M. M. Schreurs, *J. Appl. Crystallogr.*, 2003, **36**, 220.

19 SADABS, Bruker Analytical X-ray Systems, Madison WI, 1997.

20 G. M. Sheldrick, *Acta Crystallogr. A*, 2008, **64**, 112.

21 L. J. Farrugia, *J. Appl. Cryst.* 2012, **45**, 849.

22 A. D. Becke, *J. Chem. Phys.*, 1992, **96**, 2155.

23 M. J. Frisch, G. W. Trucks, H. B. Schlegel, G. E. Scuseria, M. A. Robb, J. R. Cheeseman, G. Scalmani, V. Barone, B. Mennucci, G. A. Petersson, H. Nakatsuji, M. Caricato, X. Li, H. P. Hratchian, A. F. Izmaylov, J. Bloino, G. Zheng, J. L. Sonnenberg, M. Hada, M. Ehara, K. Toyota, R. Fukuda, J. Hasegawa, M. Ishida, T. Nakajima, Y. Honda, O. Kitao, H. Nakai, T. Vreven, J. A. Montgomery Jr., J. E. Peralta, F. Ogliaro, M. Bearpark, J. J. Heyd, E. Brothers, K. N. Kudin, V. N. Staroverov, R. Kobayashi, J. Normand, K.

Raghavachari, A. Rendell, J. C. Burant, S. S. Iyengar, J. Tomasi, M. Cossi, N. Rega, J. M. Millam, M. Klene, J. E. Knox, J. B. Cross, V. Bakken, C. Adamo, J. Jaramillo, R. Gomperts, R. E. Stratmann, O. Yazyev, A. J. Austin, R. Cammi, C. Pomelli, J. W. Ochterski, R. L. Martin, K. Morokuma, V. G. Zakrzewski, G. A. Voth, P. Salvador, J. J. Dannenberg, S. Dapprich, A. D. Daniels, Ö. Farkas, J. B. Foresman, J. V. Ortiz, J. Cioslowski and D. J. Fox, *Gaussian 09*, Revision A.1, Gaussian, Inc., Wallingford, CT, 2009.

24 (*a*) T. H. Dunning Jr. and P. J. Hay, in *Methods of Electronic Structure Theory*, H. F. Schaefer III, ed., Plenum Press New York, 1977, vol. 2; (*b*) P. J. Hay and W. R. Wadt, *J. Chem. Phys.*, 1985, **82**, 270.

25 G. A. Zhurko, *ChemCraft*, http://www.chemcraftprog.com

26 M. E. Ali and S. N. Datta, *J. Phys. Chem. A*, 2006, **110**, 2776.

27 R. T. Azuah, L. R. Kneller, Y. Qiu, P. L. W. Tregenna-Piggott, C. M. Brown, J. R. D. Copley and R. M. Dimeo, *J. Res. Natl. Inst. Stan. Technol.*, 2009, **114**, 341.

28 P. L. W. Tregenna-Piggott, D. Sheptyakov, L. Keller, S. I. Klokishner, S. M. Ostrovsky, A. V. Palii, O. S. Reu, J. Bendix, T. Brock-Nannestad, K. Pedersen, H. Weihe and H. Mutka, *Inorg. Chem.*, 2009, **48**, 128.

29 A. W. Addison, T. N. Rao, J. Reedijk, J. van Rijn and G. C. Verschoor, *J. Chem. Soc., Dalton Trans*., 1984, 1349.

30 G. P. Guedes, R. G. Zorzanelli, N. M. Comerlato, N. L. Speziali, S. Santos-Jr and M. G. F. Vaz, *Inorg. Chem. Commun*., 2012, **23**, 59.

31 (*a*) M.-U.-Haque and C. N. Caughlan, *J. Chem. Soc., Perkin Trans.*, 1976, **2**, 1101; (*b*) F. Cameron and F. D. Duncanson, *Acta Crystallogr. B*, 1981, **37**, 1604; (*c*) B. Davidowitz, T. A. Modro, M. L. Niven, *Phosphorus Sulfur*, 1985, **22**, 255.

32 M. A. Voinov, T. G. Shevelev, T. V. Rybalova, Y. V. Gatilov, N. V. Pervukhina, A. B. Burdukov and I. A. Grigor'ev, *Organometallics*, 2007, **26**, 1607.

33 F. Iwasaki, J. H. Yoshikawa, H. Yamamoto, K. Takada, E. Kan-nari, M. Yasui, T. Ishida and T. Nogami. *Acta Crystallogr., Sect. B: Struct. Sci., Cryst. Eng. Mater.*, 1999, **55**, 1057.

34 M. G. F. Vaz, H. Akpinar, G. P. Guedes, S. Santos, M. A. Novak and P. M. Lahti, *New J. Chem*., 2013, **37**, 1927.

35 (*a*) R. Taylor, *CrystEngComm*, 2014, **16**, 6852; (b) K. Durka, S. Lulinski, K. N. Jarzembska, J. Smetek, J. Serwatowski and K.Wozniak,*Acta Crystallogr., Sect. B: Struct. Sci., Cryst. Eng. Mater*., 2014, **70**, 157; (c) F. F. Awwadi, R. D. Willett, K. A. Peterson and B. Twamley, *Chem. Eur. J.* 2006, **12**, 8952; (d) R. B. K. Siram, D. P. Karothu, T. N. G. Row and S. Patil, *Cryst. Growth Des.*, 2013, **13**, 1045.

36 O. Kahn, *Molecular Magnetism*, VCH, Weinheim, 1993.

37 R. L. Carlin, *Magnetochemistry*, Springer-Verlag, Berlin, 1986.

38 B. Moubaraki, K. S. Murray, T. A. Hudson and R. Robson, *Eur. J. Inorg. Chem.* 2008, **2008**, 4525.

39 A. Caneschi, D. Gatteschi, R. Sessoli, P. Rey, *Acc. Chem. Res.*, 1989, **22**, 392.

40 (*a*) G. P. Guedes, S. Soriano, N. M. Comerlato, N .L. Speziali, P. M. Lahti, M. A. Novak and M. G. F. Vaz, *Eur. J. Inorg. Chem.*, 2012, **23** 5642; (*b*) J. Titiš and R. Boča, *Inorg. Chem.*, 2011, **50**, 11838.

41 F. Lloret, M. Julve, J. Cano, R. Ruiz-Garcia, E. Pardo, *Inorg. Chim. Acta*, 2008, **361**, 3432.

42 (*a*) H. Kumada, A. Sakane, N. Koga and H. Iwamura, *J. Chem. Soc., Dalton Trans.*, 2000, 911; (*b*) W. Wojciechowski, *Inorg. Chim. Acta*, 1967, **1**, 324.

43 (*a*) M. G. F. Vaz, R. A. Allão, H. Akpinar, J. A. Schlueter, S. Santos, P. M. Lahti and M. A. Novak, *Inorg. Chem.*, 2012, **51**, 3138; (*b*) C. Rancurel, D. B. Leznoff, J.-P. Sutter, S. Golhen, L. Ouahab, J. Kliava and O. Kahn, *Inorg. Chem.*,1999, **38**, 4753.

44 M. Baskett, P. M. Lahti, A. Paduan-Filho and N. F. Oliveira, Jr., *Inorg. Chem.*, 2005, **44**, 6725.

45 (a) J. S. Huang and M. Kertesz, *J. Am. Chem. Soc.*, 2007, **129**, 1634; (b) G. P. Guedes, A. S. Florencio, J. W. M. Carneiro, M. G. F. Vaz, *Solid State Sci*., 2013, **18**, 10; (c) A. Bencini, A. Dei, C. Sangregorio, F. Totti and M. G. F. Vaz, *Inorg. Chem.*, 2003, **42**, 8065; (d) D. A. Souza, A. S. Florencio, S. Soriano, R. Calvo, R. P. Sartoris, J. W. de M. Carneiro, C. Sangregorio, M. A. Novak and M. G. F. Vaz, *Dalton Trans*., 2009, 6816.

46 (*a*) S. Nakano, Y. Kitagawa, T. Kawakami, K. Yamaguchi, *Polyhedron*, 2003, **22**, 2027; (*b*) P. Mondal, R. Singh, A. Hens, J. Cano, E. Colacio, K. K. Rajak, *Polyhedron*, 2013, **65**, 60; (*c*) F. Cimpoesu, M. Ferbinteanu, B. Frecus, M. A. Gîrtu, *Polyhedron*, 2013, **28**, 2039; (*d*) E. Ruiz, A. Rodríguez-Fortea, J. Cano, S. Álvarez, P. Alemany, *J. Comp. Chem*. 2003, **24**, 982.

47 (*a*)A. S. Florencio, R.A. Allão, M. G. F. Vaz, J. W. M. Carneiro, *Inorg. Chem. Commun.*, **2012**, *24*, 67; (*b*) R. A. Allão, A. K. Jordão, J. A. L. C. Resende, A. C. Cunha, V. F. Ferreira, M. A. Novak, C. Sangregorio, L. Sorace and M. G. F. Vaz, *Dalton Trans*., 2011, **40**, 10843.

48 (*a*) L. Jia, J.-C. Xie, J. Zhang, H.-L. Sun, Z. Li, *Inorg. Chem. Commun.*, 2012, **16**, 33; (*b*) H. Tian, Y. Li, C. Zhang, X. Mei, P. Hu, L. Li, *Polyhedron*, 2013, **52**, 1053.